

Hua Yang · Chen Zhang · Hui Zheng · Wei Xiong
Zhuan Zhou · Tao Xu · Jiu Ping Ding

A simulation study on the Ca^{2+} -independent but voltage-dependent exocytosis and endocytosis in dorsal root ganglion neurons

Received: 3 January 2005 / Revised: 23 February 2005 / Accepted: 6 April 2005 / Published online: 10 June 2005
© EBSA 2005

Abstract In patch-clamped somata of dorsal root ganglion (DRG) neurons, two types of secretion have been proposed: Ca^{2+} -dependent secretion and Ca^{2+} -independent but voltage-dependent secretion (CIVDS). The Ca^{2+} -induced and the depolarization-induced membrane capacitance (C_m) increases contribute 80 and 20% to the total C_m increase, respectively (Zhang and Zhou in *Nat Neurosci* 5:425, 2002). In order to explore the mechanism of the voltage-dependent C_m change (ΔC_m), we constructed a model with sequential states. The simulation with this model closely approximates all the experimental data. The model predicts that the majority of fusion events (approximately 80%) are so-called “kiss-and-run” events, which account for the fast recovery or the rapid retrieval feature of the signals. The remaining 20% are attributed to full fusion events, which account for a slow retrieval feature. On the basis of the model, one mechanism of the activity-dependent endocytosis has revealed a differential distribution of vesicles between the kiss-and-run and full fusion states at different stimulation frequencies. The quantitative model presented in this study may help us to understand

the mechanism of the CIVDS and the tightly coupled endocytosis found in mammalian DRG neurons.

Keywords Exocytosis · Endocytosis · Ca^{2+} -independent but voltage-dependent secretion · Capacitance · Vesicle

Introduction

The classical “ Ca^{2+} hypothesis” for neurotransmitter release has predominated in neurobiology and has provided an essential framework for understanding how excitation in nerve terminals controls transmitter release (Katz 1969; Xu et al. 1998; Voets et al. 1999). According to this hypothesis, an action potential (AP) invades the presynaptic nerve terminal and opens voltage-gated Ca^{2+} channels, resulting in a brief elevation of the intracellular Ca^{2+} concentration ($[\text{Ca}^{2+}]_i$). The transient increase in the local $[\text{Ca}^{2+}]_i$ near the fusion sites of synaptic vesicles thus triggers phasic transmitter release (Katz 1969; Llinas 1977; Augustine et al. 1987; Zucker 1996). Yet, a controversy surrounds the issue of whether an additional mechanism exists to account for the initiation of transmitter release. Evidence from various laboratories has suggested that membrane potential per se has a direct role in modulating transmitter release (Hochner et al. 1989; Mochida et al. 1998; Ben-Chaim et al. 2003). Membrane depolarization can cause transmitter release when Ca^{2+} entry is blocked and intracellular $[\text{Ca}^{2+}]_i$ levels are held at an elevated level (Silinsky et al. 1995). In addition to membrane potentials, it has been suggested that various stimuli can trigger exocytosis in a Ca^{2+} -independent manner, such as via $\text{GTP}\gamma\text{S}$, PMA and certain G-protein-coupled receptors (Hirose et al. 1997; Iino et al. 2000; Zhu et al. 2002). On the other hand, Parnas et al. (2002) constructed a mathematical model to reconcile the Ca^{2+} hypothesis and the Ca^{2+} and voltage hypothesis for transmitter release. In their model, both the Ca^{2+} and

H. Yang · T. Xu · J. P. Ding (✉)
Institute of Biophysics and Biochemistry,
College of Life Science and Technology,
Huazhong University of Science and Technology,
Wuhan, 430074, China
E-mail: jpding@mail.hust.edu.cn
Tel.: +86-27-87464577
Fax: +86-27-87464577

T. Xu
National Laboratory of Biomacromolecules,
Institute of Biophysics, Chinese Academy of Sciences,
Shanghai, 200031, China

H. Zheng · W. Xiong · Z. Zhou
Institute of Molecular Medicine, Peking University,
Beijing, 100871, China

C. Zhang · H. Zheng · W. Xiong · Z. Zhou
Institute of Neuroscience,
Shanghai Institutes for Biological Sciences,
Chinese Academy of Sciences, Shanghai, 200031, China

the voltage are necessary for transmitter release, although spontaneous fusion occurs at the resting potential with a very low $[Ca^{2+}]_i$.

Recently, a depolarization-induced but Ca^{2+} -independent secretion was revealed in the somata of rat dorsal root ganglion (DRG) neurons (Zhang and Zhou 2002). On the basis of membrane capacitance measurement as an assay for exocytosis, a depolarization-induced C_m increase has been revealed in the absence of extracellular Ca^{2+} and when intracellular $[Ca^{2+}]_i$ is held at a very low level with 10 mM 1,2-bis(2-aminophenoxy)ethane-*N,N,N',N'*-tetraacetic acid (BAPTA). With maximal stimulation, Ca^{2+} -independent but voltage-dependent secretion (CIVDS) contributes 20% of the total C_m increase in the presence of Ca^{2+} . More recently, amperometric and FM dye fluorescence measurements were also employed to verify that these C_m signals indeed represented exocytosis (Zhang et al. 2004). Endocytosis is critical for vesicle recycling and is known to follow stimulated exocytosis. It is generally believed that vesicle endocytosis is regulated by Ca^{2+} or is Ca^{2+} -independent, but activity-dependent (Sun et al. 2002; Wu 2004). However, recently a rapid endocytosis (RE) has been suggested to happen in the complete absence of Ca^{2+} (Zhang et al. 2004). Altogether, the unanimous discrepancy among them is that they have different triggers, such as Ca^{2+} , GTP γ S or voltage for release vesicles, even though there is a great diversity of release styles.

To understand the characteristic of the voltage-dependent C_m change, a suitable model is highly desirable. There are two aims for this study. One aim is first to derive a model that can be used to describe the experimental data of the voltage-dependent C_m signals, and to predict the underlying mechanism of the Ca^{2+} -independent exocytosis and endocytosis in the somata of DRG neurons. Another aim is to provide a clue to seek the putative voltage-sensing proteins. The CIVDS has only been found in DRG cells so far, but it may not be limited to DRG cells in the long term. In other words, it may take years to find the existence of CIVDS in other systems. This could arise for a number of reasons. First, CIVDS is usually much weaker than Ca^{2+} -dependent secretion (CDS), which might be difficult to recognize as a valid secretion. Second, CIVDS exists in cell types that contain an unknown voltage-sensing fusion protein expressed in DRG neurons. Third, it is possible that the CIVDS of cells except for a few cell types has not been extensively studied yet. The current study will help us to further validate the other types of cells with CIVDS and to understand its physiological significance. The model may also provide more valuable information for other modeling work.

Materials and methods

Cell preparation and patch-clamp recording conditions

The use and care of animals in this study followed the guidelines of the Shanghai Institutes of Biological

Sciences Animal Research Advisory Committee. Freshly isolated DRG neurons from approximately 120-g Wistar rats (SLACCAS, Shanghai) were prepared as described previously (Zhang and Zhou 2002). Dissociated cells were used 1–8 h after plating. We selected small (15–25 μ m, C-type) neurons without apparent processes. Somatic whole-cell recordings were made using pipettes of 2–4 M Ω , an EPC9/2 amplifier (HEKA Elektronik, Lambrecht/Pfalz, Germany) and Pulse software (HEKA Elektronik). The standard external solution contained 150 mM NaCl, 5 mM KCl, 2.5 mM $CaCl_2$, 10 mM *N*-(2-hydroxyethyl)piperazine-*N'*-ethanesulfonic acid (HEPES) and 10 mM glucose (pH 7.4). For a Ca^{2+} -free bath, we removed $CaCl_2$ from the external solution and added 1 mM ethylene glycol bis(2-aminoethyl ether)-*N,N,N',N'*-tetraacetic acid (EGTA). The standard internal solution contained 153 mM CsCl, 1 mM $MgCl_2$, 10 mM HEPES and 4 mM ATP (pH 7.2). All chemicals were from Sigma (St. Louis, MO, USA), except Fura-2 and Pluronic-127 (Molecular Probes, Eugene, OR, USA). We used a perfusion system to change the external solution, which had a fast exchange time (less than 100 ms) for electronic switching between seven channels (RCP-2B, INBIO, Wuhan, China; Zhang and Zhou 2002). All experiments were carried out at room temperature (22–25°C).

C_m measurements

Membrane capacitance was measured using the software lock-in module of Pulse 8.30 together with an EPC-9/2 amplifier. A 1-kHz, 40-mV peak-to-peak sinusoid was applied around a DC holding potential of –60 mV. Analysis of the resulting current used the Lindau–Neher technique (Gillis 1995; Zhang and Zhou 2002) to give estimates of C_m , membrane conductance and series resistance.

Data analysis and modeling

The differential equations for models were solved numerically, using the integration method of fourth order of Runge–Kutta. The integrating routines were written and performed with MATLAB (Mathworks, Natick, MA, USA), compiled and run on Pentium PCs. Measured data were analyzed with IgorPro (Wavemetrics, Lake Oswego, OR, USA). Statistics are given as the mean \pm the standard error of the mean. The following parameters were used for the model in Scheme 1 for all the simulations:

$$k_1 = 70e^{0.12V}, \quad k_{-1} = 0.1e^{-0.12V}, \quad k_2 = 16, \\ k_{-2} = 0.6, \quad k_3 = 0.15, \quad k_{-3} = 0.01 \text{ (unit: s}^{-1}\text{)}. \quad (1)$$

Here, the steady-state values were calculated as the initial values of the states for –60 and –80 mV:

$$\begin{aligned} \text{RRP} &= 0.8570, & \text{VAP} &= 0.0003, & \text{Exp1} &= 0.0089, \\ \text{RRP} &= 0.9986, & \text{VAP} &= 0.0000, & \text{Exp1} &= 0.0001, \end{aligned}$$

$$\begin{aligned} \text{Exp2} &= 0.1338 \quad \text{for } -60 \text{ mV}; \\ \text{Exp2} &= 0.0013 \quad \text{for } -80 \text{ mV}. \end{aligned} \quad (2)$$

Results

Voltage dependence and double-exponential decay of CIVDS

In rat DRG neurons, depolarization induces a C_m increase in the absence of extracellular Ca^{2+} and when the intracellular $[\text{Ca}^{2+}]_i$ is buffered at a very low level in the presence of 10 mM BAPTA (Zhang and Zhou 2002). Recently, using FM dye and C_m measurements, we confirmed this voltage-dependent C_m increase, and further investigated the voltage-dependent endocytosis of CIVDS (Zhang et al. 2004). First, we are going to look briefly over the data in the two papers just mentioned. A major proportion (approximately 80%) of the endocytosis is very fast, with a time constant of 0.48 s (Fig. 1). The remaining 20% of endocytosis declines slowly, with a time constant of 10.1 s. The change of C_m (ΔC_m) varies with both voltages and repolarization durations. The voltage of half-maximum ΔC_m obtained at a holding potential of -60 mV is about -22 mV (Fig. 2b). Zhang and Zhou (2002) showed the rising phase of exocytosis (Fig. 3a, solid circles) by depolarization from -60 to 0 mV with varying durations. In Fig. 3c, we present the recovery time course (solid circles) from paired-pulse experiments. The double-exponential curve of recovery indicates that there is a slow and a fast component in the recovery course. The frequency dependency of the C_m change stimulated by a train of depolarization is summarized in Fig. 4, where the accumulated effect of 40

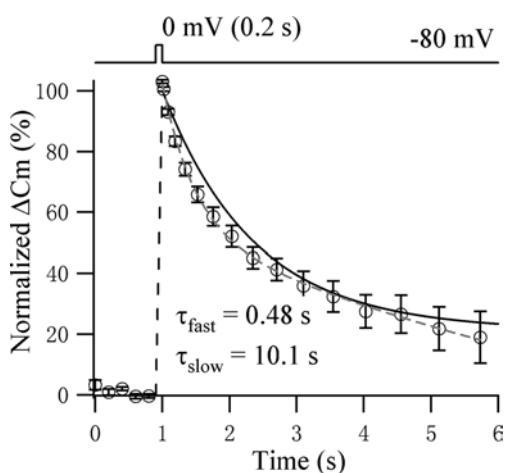


Fig. 1 Simulation of voltage-induced C_m signals in a 0-mM Ca^{2+} bath. The average trace of endocytosis (circles, $n=21$) in a Ca^{2+} -free bath was obtained using the indicated voltage protocol. The simulation result is displayed as a solid line and the double-exponential fit to data is indicated as a broken line. The fast time constant of endocytosis is $\tau_{\text{fast}}=0.48$ s (80%) and the slow time constant of endocytosis is $\tau_{\text{slow}}=10.1$ s (20%)

depolarization pulses stepping to 0 mV from a holding potential of -80 mV at frequencies of 1, 4, 10, 40 and 100 Hz is displayed (Zhang et al. 2004). An example trace for 1 Hz is shown in Fig. 4a. The symbols in Fig. 4b show the time course of endocytosis after 40-pulse depolarization. The solid symbols in Fig. 4c present the time constants and the relative steady-state values ($R_{\text{end/exo}}$) of endocytosis at different frequencies, respectively.

A model for CIVDS in DRG neurons

Our goal was to derive a kinetics model to simulate and predict the experimental data and to assist in the quantitative description of CIVDS and CIVDS-coupled endocytosis, and to help unravel the mechanism of stimulus-exocytosis coupling in DRG neurons. This model should meet the two basic features of the experimental findings: the voltage-dependent C_m increase (exocytosis) and the double-exponential decay in C_m (endocytosis). Our model started from a readily releasable pool (RRP), in which vesicles were conveyed so close to the plasma membrane as to be ready for exocytosis. In voltage-activated exocytosis, the vesicles in

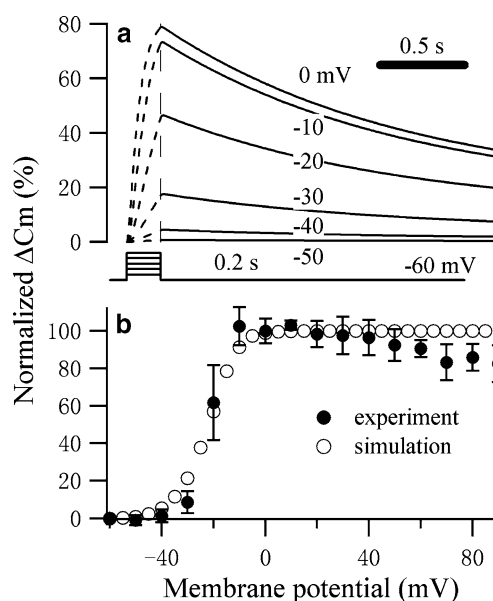


Fig. 2 Voltage dependence of Ca^{2+} -independent but voltage-dependent secretion (CIVDS) **a** The ΔC_m traces were simulated using the indicated protocol of voltage steps ranging from -50 to 0 mV in 10-mV increments from a holding potential of -60 mV. **b**, Normalized ΔC_m elicited by different voltage steps as a function of the depolarization potential (filled circles, $n=7$). Similarly, the peak values of ΔC_m in **a** are plotted (open circles) against the depolarization potential

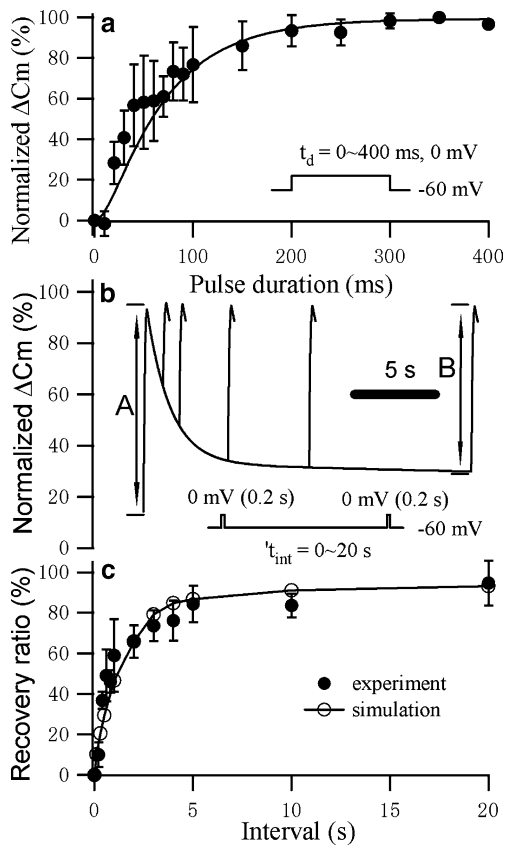


Fig. 3 Recovery of the pool sizes of CIVDS after stimulation-induced depletion. **a** ΔC_m from experiments (circles, $n=9$) and the solid line from the model are plotted as a function of the depolarization duration with the indicated protocol. **b** The recovery traces of ΔC_m calculated by the model with a paired-pulse recovery protocol, in which intervals were varied between 0 and 400 ms. The recovery ratio was defined as B/A . **c** The recovery ratio from experiments (filled circles, $n=9$) as a function of recovery duration; the solid line was calculated from the model in Scheme 1 (open circles). The double-exponential curve from experiments gives $\tau_{\text{fast}} = 0.55$ s and $\tau_{\text{slow}} = 7.54$ s

the RRP are activated first by depolarization and then merged into the plasma membrane rather than by intracellular Ca^{2+} as in the models developed by Heinemann et al. (1993, 1994). We believe that the voltage-sensitive vesicles must be already docked at the plasma membrane because the putative voltage sensor must be in the cell membrane. These voltage-sensitive vesicles must also be readily releasable and are inhibited from fusion at the resting membrane potential. They are triggered to fuse by depolarization not by Ca^{2+} . Thereby, two steps with distinct rates are involved in the previously described process, i.e., a fast voltage-activated step and a slow-fusion step. In other words, we need to add a voltage-activated pool (VAP) between the RRP and the exocytosis pool (ExP) to describe both fast and slow steps, that is, $\text{RRP} \leftrightarrow \text{VAP} \leftrightarrow \text{ExP}$. The transition rates between the RRP and the VAP are relatively large and voltage-dependent, whereas the rates between the VAP and the ExP are relatively small and voltage-independent, which is similar to the case of CDS

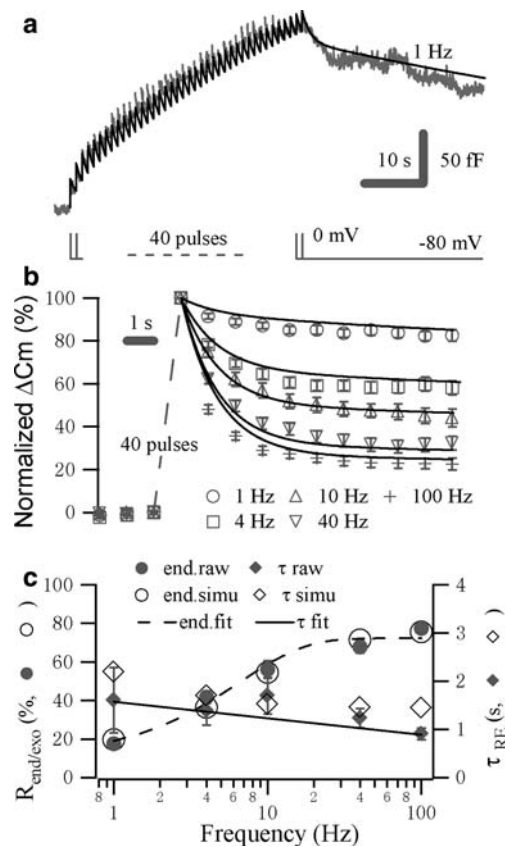
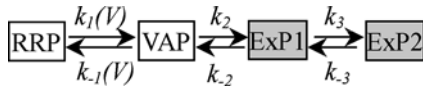


Fig. 4 Frequency dependence of CIVDS-coupled endocytosis. **a** The ΔC_m trace was evoked by depolarization with 40-pulse trains at 1 Hz (stimulation steps to 0 from -80 mV; 10-ms duration). The solid line represents the simulated trace calculated from the model. **b** Experimental data for endocytosis were normalized ($n=12$ for 1 Hz circles; $n=11$ for 4 Hz squares; $n=9$ for 10 Hz triangles; $n=20$ for 40 Hz inverted triangles; $n=11$ for 100 Hz dashes) using the protocol in **a**. The solid lines denote the normalized ΔC_m of endocytosis calculated from the model. **c** Both the fractional endocytosis of CIVDS (right, filled circles) and the decay time constant τ (left, filled diamonds) from the endocytosis experimental data in **b** as a function of frequency. Similarly, the estimates from the simulation are displayed (left, open circles; right, open diamonds). The dashed line represents a single-exponential fit of the fractional endocytosis of CIVDS (filled circles), which gives a time constant of 6.58 s. The solid line fits to the decay time constants τ (filled diamonds) with a slope of -0.0007

(Heinemann et al. 1993, 1994). The question is how to explain the endocytosis on the basis of the previously described sequential model. Because endocytosis always occurs during repolarization in our cases, we can expect that exocytosis goes forward along the transition path $\text{RRP} \rightarrow \text{VAP} \rightarrow \text{ExP}$ during depolarization, whereas endocytosis goes directly backward along the path $\text{ExP} \rightarrow \text{VAP} \rightarrow \text{RRP}$ during repolarization, which bears an analogy to ion channels. In addition, considering two distinct decay-time courses involved in endocytosis, we added the slowest ExP, ExP2, in series just behind ExP1. Finally, we constructed the CIVDS model indicated by Scheme 1, which is somehow similar to a calcium-activated model (Wang et al. 2003). Obviously, the model in Scheme 1 meets the two basic features of the experi-



Scheme 1 Model of Ca^{2+} -independent but voltage-dependent secretion. *RRP* readily releasable pool, *VAP* voltage-activated pool, *ExP* exocytosis pool

mental findings: the voltage-dependent C_m increase (exocytosis) and the double-exponential decay in C_m (endocytosis).

On the basis of the model in Scheme 1, a vesicle from an inactivated RRP to a release ExP must pass an activated VAP by membrane depolarization. $k_1(V)$ and $k_{-1}(V)$ are the forward and backward rate constants between the RRP and the VAP, respectively. According to the Eyring rate theory, $k_1(V) = k_1(0) \exp(qV)$ and $k_{-1}(V) = k_{-1}(0) \exp(-qV)$ (Eyring 1935), where $q = z_g e / k_B T$, z_g is the number of the gating charge, e is the elementary charge, k_B is Boltzmann's constant and T is the absolute temperature. The other voltage-dependent rates, k_2 , k_{-2} , k_3 and k_{-3} , are adopted to depict transitions among the VAP, ExP1 and ExP2. In contrast to models of the CDS (Heinemann et al. 1993), we did not design a multistep voltage-dependent model for two reasons. One reason is that the major discrepancy between them occurs only in the rising phase, and the second is that we cannot determine how many steps in Scheme 1 are included in CIVDS until we directly obtain the complete rising traces. In addition, we did not place an endocytosis pool (EnP) at the position of ExP2, because it brought in a very slow recovery against the data shown in Fig. 3c. The cause is that the EnP acting as a “close state” cannot provide sufficient vesicles/capacitance for a fast recovery as shown in Fig. 3c.

For a rough estimation of rates, we took a steady-state approximation to the data presented in Fig. 2b, even though the capacitances at each voltages have not reached their steady-state values yet. At equilibrium, the occupancy O of the ExPs (or the steady-state activation) is given by

$$O = \frac{1 + k_{-3}/k_3}{1 + k_{-3}/k_3 + k_{-2}k_{-3}/(k_2k_3) + k_{-1}k_{-2}k_{-3}/(k_1k_2k_3)}. \quad (3)$$

Assuming that $k_2/k_{-2} \gg 1$, $k_3/k_{-3} \gg 1$ and $k_{-1}/k_1 = k_{-1}(0)/k_1(0) \exp(-2qV)$, we rewrite Eq. 3 as follows:

$$O = 1 / \left(1 + e^{-2q(V-V_{50})} \right). \quad (4)$$

Here, $2q$ represents the reciprocal of the slope of the curve of occupancy versus voltage and V_{50} is the voltage of half-maximum occupancy. Fitting the data of the normalized ΔC_m versus voltage in Fig. 2b to Eq. 3, we obtained $q = 0.12 \text{ mV}^{-1}$ and $V_{50} = -22 \text{ mV}$. We found that $q = 0.12$ was an invariable value during the simulation, whereas other rates needed to be readjusted on the basis of the rising-time or decay-time constants.

When measuring the capacitance of DRG cells, the apparent capacitance of a cell depends on the membrane potential (data not shown). Therefore, it is very important to calculate the initial value of each pool at every holding potential. At equilibrium, the mean frequency of the forward transitions is identical to the mean frequency of the backward transitions in every elementary step—the principle of detailed balances. According to this principle, all initial values at -60 and -80 mV were calculated and are listed in “Materials and methods.” Owing to the immeasurability of the initial value of the capacitance, we subtracted the initial values for all the calculations of the capacitance.

Simulation of CIVDS under various voltage stimulations

In simulations, the number of vesicles of a pool comes from the occupancy or probability of a pool multiplied by the total number of vesicles. If the average capacitance of a vesicle is 0.5 fF (Zhang et al. 1995), the capacitance of a state or pool is obtained by multiplying the numbers of vesicle in a pool by 0.5 . According to Zhang and Zhou (2002), a depolarization step from -60 to 0 mV induces a ΔC_m of 200 fF , which corresponds to 80% of the total CIVDS (Fig. 2b) or 500 vesicles. Thus, the RRP of CIVDS is estimated to be 250 fF . In our simulation, the initial RRP size was assigned to be 1 at -80 mV , i.e., 250 fF , which means that the simulated pool size corresponds to the fraction of the CIVDS rather than an actual “pool size.”

Figure 1 shows an average trace of ΔC_m in response to a repolarization step to -80 mV following a test pulse to 0 mV in the absence of Ca^{2+} . On the basis of the parameters shown in the “Materials and methods,” the simulated curve (solid line) calculated from the model in Scheme 1 is approximately consistent with the double-exponential data (circles). If we removed the ExP2 from the model in Scheme 1, ΔC_m would return to the initial value or to zero within a time scale about $1/k_{-2} = 1.67 \text{ s}$ at -80 mV , because the whole process of endocytosis only depends on both the rates $k_{-1}(-80) = 1,476 \text{ s}^{-1}$ and $k_{-2} = 0.6 \text{ s}^{-1}$. Consequently, ExP2 plays a key role in soaking up more vesicles for a full fusion so as to maintain a higher level of ΔC_m during the longer repolarization.

To examine the voltage dependence of the ΔC_m increase, we employed a voltage protocol as indicated in Fig. 2a. Each test pulse was 200 ms in duration and the depolarization voltages were stepped from -50 to 0 mV in 10-mV increments. The pulse-induced ΔC_m was steeply voltage dependent, with half-maximal activation at a membrane potential of around -20 mV and saturation at 0 mV or higher (filled circles in Fig. 2b, from Zhang and Zhou 2002). The simulated-capacitance traces are shown in Fig. 2a and the predicted normalized ΔC_m versus the depolarization potential is plotted in Fig. 2b (open circles). From Fig. 2a, we can see that it takes

much longer than 200 ms for a trace or ΔC_m to reach a steady-state level especially at lower depolarization voltages. From Fig. 2b, we found that the slope $q=0.12$ was not a bad expectation. On the basis of the simulation results shown in Fig. 2a, we expect that the onset time constants of exocytosis will decrease with the augmentation of depolarization potentials, and that the decay time constants of endocytosis will be invariable, while the membrane potentials return to the resting potential -60 mV during endocytosis.

The RRP size of CIVDS was estimated by measuring ΔC_m in response to the depolarization for various durations (Gillis et al. 1996). We found that ΔC_m increased progressively to a saturation level with longer pulses (circles in Fig. 3a, from Zhang and Zhou 2002), which was mimicked by the model in Scheme 1 (Fig. 3a, solid line). There is no clear delay time to be seen at the root of the rising course, so we decided to choose a model with one-step voltage activation in this study.

We measured the refilling time course after depletion of CIVDS by applying a paired-pulse depolarization at variable time intervals, which were stepped to 0 from 60 mV for 200 ms (Fig. 3b) (Voets et al. 1999). The recovery of CIVDS pools was defined as the ratio of the two ΔC_m evoked by the dual pulses shown in Fig. 3b. In Fig. 3c, the filled circles indicate the refilling time course of the vesicles (Zhang and Zhou 2002) and the solid line shows the results from simulation using the model in Scheme 1. The trace of endocytosis in Fig. 3b will asymptotically reach its initial value after a longer time, because we adopted the steady-state values as the initial values. The recovery of the depleted RRP has two components, i.e., $\tau_{r-fast}=0.55$ s and $\tau_{r-slow}=7.5$ s. The fast recovery was derived from ExP1 and the slow one from ExP2. The fast fusion/retrieve between the VAP and ExP1 was induced by a rapid reuse of vesicles and the slow fusion/retrieve between ExP1 and ExP2 was caused by a complete collapse of the vesicles to the plasma membrane.

So far, we found two processes, i.e., a rapid reuse of vesicles and a full fusion, involved in CIVDS. Is there any similarity between the CIVDS and the CDS? The “classical” model of a synaptic vesicle fusion assumes a complete collapse of a vesicle into the plasma membrane and subsequent maintenance of vesicle pools requires clathrin-dependent endocytosis and membrane recycling (Richards et al. 2003). Recent evidence indicates that vesicles in central synapses fuse multiple times in quick succession in a manner called “kiss and run” (Sudhof 2000; Harata et al. 2001; Leenders et al. 2002; Tsuboi and Rutter 2003). Accordingly, we define the rapid-reuse process as “kiss and run” and the slow-fusion process as “full fusion” in this study.

Frequency-dependent endocytosis

Frequency-dependent experiments usually reflect accumulated effects of a single action. Even though a model

could explain a single response induced by one action very well, it might depict results that arise from the repeated actions very poorly. It is very important for us to verify our models with frequency-dependent experiments.

In the absence of Ca^{2+} , a train of APs, or AP-like-pulses (10-ms duration), triggers a gradual increase in C_m followed by a typical biphasic endocytosis. The CIVDS was induced by 40 AP-like-pulses at 1 Hz (Fig. 4a). On the basis of the model in Scheme 1, the simulated results agree well with the experimental data. Interestingly, we found that the endocytosis following CIVDS was highly frequency dependent. Aligning ΔC_m responses induced by 40 AP-like-pulses at 1, 4, 10, 40 and 100 Hz, we could compare the kinetics of CIVDS-coupled endocytosis (Fig. 4b). It is obvious from the figure that higher frequencies trigger more RE; for example, a train of 1 and 100 Hz induced RE of $17 \pm 3\%$ and $77 \pm 3\%$ of the preceding CIVDS, respectively (Fig. 4c, left). The model in Scheme 1 predicted this feature without any adjustment of the parameters (Fig. 4b). During simulation, we noted that ExP1 filled quickly on depolarization and about 80% of ExP1 recycled to the VAP thereafter. The 20% of the ExP1 then proceeds slowly to ExP2, which is retrieved on an even slower time scale. For higher-frequency stimulation, there is a rapid increase in ExP1 and a slower increase in ExP2, owing to inefficient transfer between them. Thus, a larger fraction of RE from ExP1 is expected. However, for lower-frequency stimulation, a larger proportion of ExP1 is removed during the inter-stimulation interval and there is a gradual build up of ExP2; hence, we observed a smaller RE and a larger slow endocytosis from ExP2 (Fig. 4b). The model in Scheme 1 also predicted that the decay time constant of endocytosis was not so dependent on the stimulation frequency, as demonstrated in the experimental measurements (Fig. 4c, right).

The CIVDS-coupled endocytosis is inhibited by 200 μ M H-7, a preferential protein kinase A (PKA) inhibitor (Zhang et al. 2004). To accommodate this effect, we can either decrease rate k_2 from ExP1 to the VAP or increase rate k_3 from ExP1 to ExP2, since the residency time or dwell time of RE (ExP1) is $1/(k_2+k_3)$. In Fig. 5, we noted a faster decay with a much higher sustained level following H-7 treatment. Therefore, we reasoned that an increase in k_3 from 0.15 to 0.5 would suffice to explain the effect of H-7 on endocytosis without changing other kinetics features of exocytosis (Fig. 5). In conclusion, the PKA inhibitor H-7 plays a role in accelerating vesicles into the full fusion pool ExP2.

A prediction of the voltage-dependent rising course

To further verify the predictability of the model, we made a prediction for the voltage dependency of the ΔC_m responses to different depolarization pulses as we mentioned before. Then, corresponding experiments

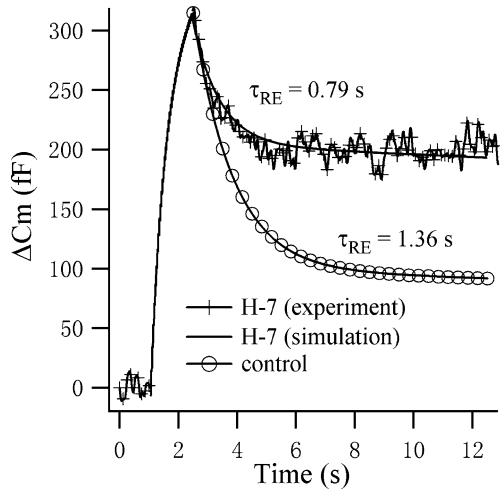


Fig. 5 Inhibition of intracellular phosphorylation affects endocytosis. Simulation from the model in Scheme 1 with an increased rate $k_3 = 0.5$ (solid line) superimposed on the averaged ΔC_m trace in response to 40-Hz depolarizing trains (crosses), which was recorded after treatment with 200 μM H-7 for 1 min ($n = 19$). The control endocytosis (circles, $k_3 = 0.15$) created by 40-Hz pulses from the model in Scheme 1 is displayed for comparison

similar to those providing the data for Fig. 3a were conducted and the results were compared with the prediction. As shown in Fig. 6, the measured data points from a depolarization to -20 mV not to 0 mV match our prediction line. We noted that the responses were quite different from those shown in Fig. 3a, where the depolarization was stepped to 0 from -60 mV. The onset rate of ΔC_m was highly dependent on the voltages, with exponential rates of 5.2 s^{-1} (Fig. 6) and 18 s^{-1} (Fig. 3a) at -20 and 0 mV, respectively. Actually, we can find an approximate formula to describe the onset process. During depolarization, the onset of ΔC_m

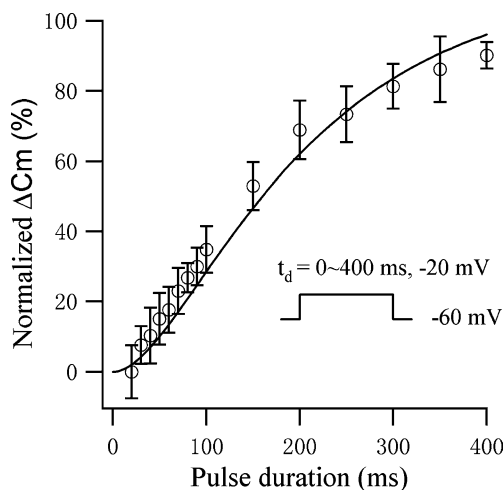


Fig. 6 Experimental verification of a prediction by the CIVDS model. ΔC_m from experiments (circles, $n = 4$) and from the model in Scheme 1 (solid line) as a function of the depolarization duration with the indicated protocol, in which the voltage was stepped from -60 to -20 mV with varying durations

is mainly dependent on the forward process of $\text{RRP} \rightarrow \text{VAP} \rightarrow \text{ExP1}$, which can be described as

$$O_{\text{rise}}(t) = 1 - k_2 \exp(-k_1 t) / (k_2 - k_1) - k_1 \exp(-k_2 t) / (k_1 - k_2). \quad (5)$$

Here, O_{rise} represents the occupancy of ExP1 during depolarization. If we let the integral of the sum of the two exponential components in Eq. 5 equal that of a single exponential, we get

$$\int_0^{\infty} (k_2 e^{-k_1 t / (k_2 - k_1)} + k_1 e^{-k_2 t / (k_1 - k_2)}) dx = \int_0^{\infty} a e^{-b t} dt, \quad (6)$$

where $a = k_1 + k_2$.

From Eq. 6, the double-exponential equation can be further simplified to a single-exponential with a rate constant b (or k_{rise}):

$$k_{\text{rise}} = k_1 k_2 / (k_1 + k_2). \quad (7)$$

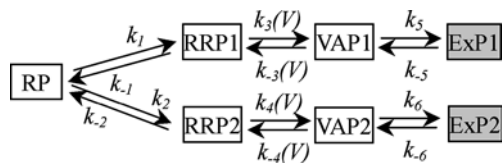
According to Eq. 7, the predicted rates for the ΔC_m increase were 13.0 and 4.5 s^{-1} at membrane potentials of -20 and 0 mV, respectively, which was in agreement with the measured data.

Our present model was derived from experimental data (Zhang and Zhou 2002; Zhang et al. 2004), from experiments in which we had investigated not only the curve of the probability of secretion versus voltage, but also included the rise, decay and their combined processes, such as recovery and train depolarization. In spite of its simplification, the model predicts a large range of phenomena and should be helpful in further elucidating the nature of voltage-dependent exocytosis. Obviously, it is necessary to design better experiments or adopt new techniques so as to refine the current model.

Other possible models of CIVDS

As for modeling work, we can always find more than one model which can be used to explain the same data. Usually, we evaluate a model by its rationality, simplicity, accuracy and predictability concerning the data in our possession. The model in Scheme 1 is a rational, simple model with strong predictability. Compared with other possible models of CIVDS such as a revised model of that in Scheme 1 composed of two ExPs in parallel, we did not find any visible difference in depicting the data of CIVDS (the results of the simulation are not shown here).

Here, we show a more complex model with two RRP in parallel (Scheme 2) which could equally simulate the data of CIVDS. Actually, the two endocytic recycling routes that selectively fill two vesicle pools in frog motor nerve terminals have been suggested (Richards et al. 2000). The ‘‘shortcoming’’ of the model is that the model in Scheme 2 behaves more like the sum of two individual models with more free parameters, because the rates between a reserve pool (RP) and a RRP are adopted



Scheme 2 Model with two RRP in parallel. *RP* reserve pool

typically extremely low and can be ignored (Heinemann et al. 1994). We find that either a series or a parallel model can work for CIVDS in DRG cells; however, we do not have evidence to select one over the other.

As mentioned before, we restricted our analysis to a sequential model with one voltage step in this study. The one-step model can be easily expanded to a multistep model with no significant difference except the slower rising phase of exocytosis (simulation data not shown here). However, we can infer that any successful model for CIVDS should share a common structure, that is, it should have a “voltage-dependent core,” i.e., $\text{RRP} \leftrightarrow \text{VAP}$, with two retrieve pathways in the models.

Discussion

There has been controversy over voltage-dependent secretion for a long time. It would be interesting to know if there is a suitable model for CIVDS. Our aims were to explore how well a model can describe this phenomenon and what clues can be used to seek for the voltage-sensing protein of CIVDS (Silinsky et al. 1995; Mochida et al. 1998; Ben-Chaim et al. 2003). On the basis of the experimental data of Ca^{2+} -independent and voltage-induced C_m increase with its subsequent decay, we proposed a novel model composed of the sequential vesicle pools in the present study. The model successfully simulated all of the experimental data, including depolarization-induced CIVDS and subsequent endocytosis, the voltage dependence, the fast recovery of CIVDS and the frequency-dependent feature of endocytosis. With the aid of the present model, further experiments precisely designed would become much easier.

A putative voltage sensor of CIVDS

Signals other than Ca^{2+} triggering for exocytosis have been elusive and intriguing for a long time. This depolarization-induced C_m increase has been regarded as providing direct evidence for a triggering role of voltage in exocytosis. The voltage sensor of CIVDS remains to be identified. It has been suggested that the core complex required for triggering membrane fusion is inhibited under resting conditions (Slutsky et al. 1999; Bradley et al. 2000; Parnas et al. 2002). It is possible that a voltage-induced conformational change associated with the core complex could also help to remove the inhibition and trigger exocytosis. In fact, Parnas et al. (2002)

created such a mathematical model in which both the Ca^{2+} and the voltage are necessary for transmitter release. The key role of the SNARE complex and synaptotagmins in triggering Ca^{2+} -dependent exocytosis has been firmly established (Jahn et al. 2003). Therefore, if there is voltage-induced membrane fusion, it is likely that the putative voltage sensor is associated with proteins such as the SNARE complex and synaptotagmins. The association of a SNARE complex has been demonstrated for voltage-dependent Ca^{2+} channels (Sheng et al. 1996). Indeed, the voltage-sensing protein has been previously suggested to be the N-type Ca^{2+} channels (Mochida et al. 1998; Sheng et al. 1996). Here, the Ca^{2+} channel serves two roles: as a voltage sensor and as a conventional Ca^{2+} channel. More recently, Ben-Chaim (2003) found that the M_2 muscarinic G-protein-coupled receptor is a voltage-sensing protein for the release of Ach (Slutsky et al. 1999). In Fig. 2b, the normalized ΔC_m has a limited slope $1/(2q)$ of e -fold per 4.2 mV and $V_{50} = -22$ mV. Therefore, the equivalent gating charge z_g for exocytosis is approximately 6.3 elementary charges. This means that a single subunit of unknown fusion proteins contains approximately 1.6 charges, if we suppose that there are four subunits in total. The gating properties of the unknown fusion proteins are similar to the kinetics characteristics of a voltage-gated ion channel, i.e., T-type calcium channel, because a T-type calcium channel has a relative negative $V_{50} = -46$ mV (Klockner et al. 1999) and $z_g \approx 8 \sim 12$.

Kiss and run and CIVDS

In a recent study, Tsien's group (Aravanis et al. 2003) detected single vesicle release in synapses at different frequencies of stimulation using fluorescence imaging. They found that most vesicles (85%) lost only a portion of their total dye during a single fusion event, but were able to fuse again soon thereafter. They interpreted these as kiss-and-run events too, with a lifetime of less than 1.4 s, followed by rapid reuse. Only 15% of the fusion events were consistent with a classical picture of exocytosis, or a complete release of FM dye from the fused vesicle. This mechanism permits fast local reuse of vesicles to support multiple neurotransmission events. In our model, the fast reversible transition between ExP1 and the VAP constitutes the RE and the fast recovery feature, which is consistent with the kiss-and-run mode and constitutes 80% of the voltage-induced Ca^{2+} -independent exocytosis. The 20% of vesicles in ExP1 were transitioned reversibly to the full fusion state (ExP2), whereas the slow pathway from ExP2 back to the RRP represents the residual 20% of slow endocytosis arising from full fusion. This is in good agreement with the finding in synapses in the presence of Ca^{2+} from Tsien's group. The estimated lifetimes of vesicles in kiss-and-run events and the kinetics of the slow endocytosis are also consistent with those of previous studies. Thus, the voltage-induced Ca^{2+} -independent exocytosis in the

somata of DRG neurons seems to share properties with Ca^{2+} -dependent transmitter release in synapses.

Activity dependence of endocytosis

Our model provides a previously overlooked explanation for frequency-dependent endocytosis, in which different frequencies of stimulation may alter the dynamic distribution of vesicles between kiss-and-run and full fusion states. At higher AP frequencies, a larger fraction of vesicles transits into the kiss-and-run fusion state and a smaller proportion into the full fusion state. In other words, a larger fraction of RE would be expected at higher stimulation frequency. Consequently, our model reveals the intrinsic essence of frequency-dependent endocytosis of CIVDS occurred in DRG neurons.

Acknowledgements We thank Chris Lingle, Steven Mennerick and Iain Bruce for comments on the manuscript. This work was supported by grants from the National Science Foundation of China (30025023, 3000062 30130230, 30328013 and 30330210), the Major State Basic Research Program of the P.R. China (G1999054000, 2001CCA04100 and G2000077800), the Li Foundation and the Sinogerman Scientific Center.

References

- Aravanis AM, Pyle JL, Harata NC, Tsien RW (2003) Imaging single synaptic vesicles undergoing repeated fusion events: kissing, running, and kissing again. *Neuropharmacology* 45:797–813
- Augustine GJ, Charlton MP, Smith SJ (1987) Calcium action in synaptic transmitter release. *Annu Rev Neurosci* 10:633–693
- Ben Chaim Y, Tour O, Dascal N, Parnas I, Parnas H (2003) The M2 muscarinic G-protein-coupled receptor is voltage-sensitive. *J Biol Chem* 278:22482–22491
- Bradley SR, Marino MJ, Wittmann M, Rouse ST, Awad H, Levey AI, Conn PJ (2000) Activation of group II metabotropic glutamate receptors inhibits synaptic excitation of the substantia nigra pars reticulata. *J Neurosci* 20:3085–3094
- Eyring (1935) Ionic channels of excitable membranes. Book
- Gillis KD (1995) Techniques for membrane capacitance measurements. In: *Single channel recording*, 2nd edn. pp 155–198
- Gillis KD, Mossner R, Neher E (1996) Protein kinase C enhances exocytosis from chromaffin cells by increasing the size of the readily releasable pool of secretory granules. *Neuron* 16:1209–1220
- Harata N, Pyle JL, Aravanis AM, Mozhayeva M, Kavalali ET, Tsien RW (2001) Limited numbers of recycling vesicles in small CNS nerve terminals: implications for neural signaling and vesicular cycling. *Trends Neurosci* 24:637–643
- Heinemann C, von Ruden L, Chow RH, Neher E (1993) A two-step model of secretion control in neuroendocrine cells. *Pflügers Arch* 424:105–112
- Heinemann C, Chow RH, Neher E, Zucker RS (1994) Kinetics of the secretory response in bovine chromaffin cells following flash photolysis of caged Ca^{2+} . *Biophys J* 67:2546–2557
- Hirose H, Seto Y, Maruyama H, Dan K, Nakamura K, Saruta T (1997) Effects of alpha 2-adrenergic agonism, imidazolines, and G-protein on insulin secretion in beta cells. *Metabolism* 46:1146–1149
- Hochner B, Parnas H, Parnas I (1989) Membrane depolarization evokes neurotransmitter release in the absence of calcium entry. *Nature* 342:433–435
- Iino S, Sudo T, Niwa T, Fukasawa T, Hidaka H, Niki I (2000) Annexin XI may be involved in Ca^{2+} - or GTP-gammaS-induced insulin secretion in the pancreatic beta-cell. *FEBS Lett* 479:46–50
- Jahn R, Lang T, Sudhof TC (2003) Membrane fusion. *Cell* 112:519–533
- Katz B (1969) The release of neural transmitter substances. Thomas, Springfield
- Klockner U, Lee JH, Cribbs LL, Daud A, Hescheler J, Perezverzev A, Perez-Reyes E, Schneider T (1999) Comparison of the Ca^{2+} currents induced by expression of three cloned alpha1 subunits, alpha1G, alpha1H and alpha1I, of low-voltage-activated T-type Ca^{2+} channels. *Eur J Neurosci* 11:4171–4178
- Leenders AG, Scholten G, de Lange RP, Lopes da Silva FH, Ghijsen WE (2002) Sequential changes in synaptic vesicle pools and endosome-like organelles during depolarization near the active zone of central nerve terminals. *Neuroscience* 109:195–206
- Llinas RR (1977) Depolarization-release coupling systems in neurons. *Neurosci Res Program Bull* 15:555–687
- Mochida S, Yokoyama CT, Kim DK, Itoh K, Catterall WA (1998) Evidence for a voltage-dependent enhancement of neurotransmitter release mediated via the synaptic protein interaction site of N-type Ca^{2+} channels. *Proc Natl Acad Sci USA* 95:14523–14528
- Parnas H, Valle-Lisboa JC, Segel LA (2002) Can the Ca^{2+} hypothesis and the Ca^{2+} -voltage hypothesis for neurotransmitter release be reconciled? *Proc Natl Acad Sci USA* 99:17149–17154
- Richards DA, Guatimosim C, Betz WJ (2000) Two endocytic recycling routes selectively fill two vesicle pools in frog motor nerve terminals. *Neuron* 27:551–559
- Richards DA, Guatimosim C, Rizzoli SO, Betz WJ (2003) Synaptic vesicle pools at the frog neuromuscular junction. *Neuron* 39:529–541
- Sheng ZH, Rettig J, Cook T, Catterall WA (1996) Calcium-dependent interaction of N-type calcium channels with the synaptic core complex. *Nature* 379:451–454
- Silinsky EM, Watanabe M, Redman RS, Qiu R, Hirsh JK, Hunt JM, Solsona CS, Alford S, MacDonald RC (1995) Neurotransmitter release evoked by nerve impulses without Ca^{2+} entry through Ca^{2+} channels in frog motor nerve endings. *J Physiol* 482(Pt 3):511–520
- Slutsky I, Parnas H, Parnas I (1999) Presynaptic effects of muscarine on ACh release at the frog neuromuscular junction. *J Physiol* 514(Pt 3):769–782
- Sudhof TC (2000) The synaptic vesicle cycle revisited. *Neuron* 28:317–320
- Sun JY, Wu XS, Wu LG (2002) Single and multiple vesicle fusion induce different rates of endocytosis at a central synapse. *Nature* 417:555–559
- Tsuboi T, Rutter GA (2003) Insulin secretion by ‘kiss-and-run’ exocytosis in clonal pancreatic islet beta-cells. *Biochem Soc Trans* 31:833–836
- Voets T, Neher E, Moser T (1999) Mechanisms underlying phasic and sustained secretion in chromaffin cells from mouse adrenal slices. *Neuron* 23:607–615
- Wang CT, Lu JC, Bai J, Chang PY, Martin TF, Chapman ER, Jackson MB (2003) Different domains of synaptotagmin control the choice between kiss-and-run and full fusion. *Nature* 424:943–947
- Wu LG (2004) Kinetic regulation of vesicle endocytosis at synapses. *Trends Neurosci* 27:548–554
- Xu T, Binz T, Niemann H, Neher E (1998) Multiple kinetic components of exocytosis distinguished by neurotoxin sensitivity. *Nat Neurosci* 1:192–200
- Zhang C, Zhou Z (2002) Ca^{2+} -independent but voltage-dependent secretion in mammalian dorsal root ganglion neurons. *Nat Neurosci* 5:425–430
- Zhang X, Aman K, Hokfelt T (1995) Secretory pathways of neuropeptides in rat lumbar dorsal root ganglion neu-

- rons and effects of peripheral axotomy. *J Comp Neurol* 352:481–500
- Zhang C, Xiong W, Zheng H, Wang L, Lu B, Zhou Z (2004) Calcium- and dynamin-independent endocytosis in dorsal root ganglion neurons. *Neuron* 42:225–236
- Zhu HL, Hille B, Xu T (2002) Sensitization of regulated exocytosis by protein kinase C. *Proc Natl Acad Sci USA* 99:17055–17059
- Zucker RS (1996) Exocytosis: a molecular and physiological perspective. *Neuron* 17:1049–1055